Journal of Power Sources 196 (2011) 6772–6780

Contents lists available at ScienceDirect

Journal of Power Sources

journal homepage: www.elsevier.com/locate/jpowsour

Electrochemical characterizations of multi-layer and composite silicon–germanium anodes for Li-ion batteries using magnetron sputtering

Chang-Mook Hwang, Jong-Wan Park*

Department of Materials Science and Engineering, Hanyang University, 17 Haengdang-dong, Seongdong-gu, Seoul 133-791, Republic of Korea

ARTICLE INFO

Article history:
Received 23 August 2010
Received in revised form 20 October 2010
Accepted 20 October 2010
Available online 2 November 2010

Key words:
Silicon
Germanium
Anode
Multilayer
Composite
Lithium-ion batteries

ABSTRACT

To improve the electrochemical performance of Si film, we investigate the addition of two film forms of Ge. Si/Ge multi-layered and Si–Ge composite electrodes that are fabricated by magnetron sputtering onto Cu current collector substrates are investigated. X-ray diffraction (XRD), scanning electron microscopy (SEM), high-resolution transmission electron microscopy (HRTEM), and extended X-ray absorption fine structure (EXAFS) are employed to analyze the structures of the Si–Ge electrodes. When used as an anode electrode for a lithium ion battery, the first discharge capacity of a Si/Ge 150 multi-layer cell with a ratio of Si 15 nm/Ge 3 nm is 2099 mAh g^{-1} between 1.1 and 0.01 V. A stable reversible capacity of 1559 mAh g^{-1} is maintained after 100 cycles with a capacity retention rate of 74.25%. Additionally, the $Si_{0.84}Ge_{0.16}$ composite has an initial discharge capacity of 1915 mAh g^{-1} and a capacity retention of 74.25%. In full cell tests of Si–Ge electrodes, the $Si_{0.84}Ge_{0.16}/LiCoO_2$ cell delivers a specific capacity of approximately 160 mAh g^{-1} and a capacity retention of 52.4% after 100 cycles. The results reveal that these two systems of sputtered Si–Ge electrodes can be used as anodes in lithium ion batteries with higher energy densities.

1. Introduction

Due to the miniaturization of portable electronics and the advent of new applications in hybrid-electric vehicles (HEVs), modern lithium ion batteries require anode materials that yield much higher specific capacities than traditional graphite anodes (theoretical capacity of 372 mAh g^{-1}) [1]. Many new materials, especially materials that form alloys with lithium (for example, Si, Sn, Ge, and Al) have shown high capacity values, sometimes having more than four Li atoms per active material atom. Among them, Si is the most attractive candidate to replace graphite due to its high theoretical specific capacity (approximately 4200 mAh g^{-1} for $Li_{22}Si_5$).

Si-based anode materials, with their characteristically high specific capacities, undergo volume expansion and contraction during electrochemical cycling due to the repeated alloying and de-alloying of Si with lithium ions that form an inter-metallic or amorphous phase containing high lithium content. Thus, their capacities fade rapidly during cycling [2,3].

Of the lithium alloys, Ge shows high capacities and has good cyclability, although it undergoes volume change like Si. The analogous Li_xGe system has received little attention. Fully lithiated $Li_{4.4}Ge$ has a high theoretical capacity of 1600 mAh g^{-1} and undergoes a volume change of 370%. The room temperature diffusivity of Li in Ge is 400 times greater than that in Si, indicating that Ge may be an attractive electrode material for high power-rate anodes [4]. However, Ge has received little attention due to its cost.

There are several ways to overcome the volume exchange problem, such as decreasing size of the structures to nano-size [5], using composites with active/active [6] or active/inactive matrixes [7], or using thin films or alloys [8]. Maranchi et al. reported that 1 μm Si films deposited by radio-frequency magnetron sputtering exhibited reversible capacities of approximately 3000 mAh g^{-1} for 12 cycles [9]. Our previous studies have described work performed on Si–Mo (active–inactive materials) binary multilayer [10] or composite systems [11]. This composite and multi-layered structure design is advantageous because of its ease of fabrication, as compared to previously studied nano-wires and 3D nano-particles. Fabrication is faster and easier using RF/DC magnetron sputtering.

In this work, Si and Ge electrodes were deposited by RF/DC magnetron sputtering, and each electrode consists of these two elements. The Si–Ge electrodes were deposited by two methods: the sequential method and co-sputter methods. (1) The Si/Ge multilayers were deposited as alternating layers stacked one by one to 90, 120, 150 Si and Ge layers. (2) The Si–Ge composite electrodes were deposited with various contents of each element by a co-sputtering system. The goals of this paper are to investigate the electrochemi-

* Corresponding author. Tel.: +82 2 2220 0386; fax: +82 2 2298 2850.
E-mail addresses: mook@hanyang.ac.kr (C.-M. Hwang), jwpark@hanyang.ac.kr (J.-W. Park).

0378-7753/$ – see front matter © 2010 Elsevier B.V. All rights reserved.
doi:10.1016/j.jpowsour.2010.10.061

cal behaviors of the Si–Ge materials and to discuss them in relation to the two systems.

We investigated the electrochemical properties of Si–Ge electrodes in an attempt to overcome the problems of single-phase Si electrodes. We confirmed that Si–Ge nano-structure (nano-composite and nano-multilayer) electrodes prepared by sputtering showed better cycle retention than the active material alone as the anode of Li-ion batteries. To identify the possibility of using active material as anodes, cell tests were performed on both half and full cells. It may be possible to find anode materials with high capacities and improved capacity retentions.

2. Experiment

Si–Ge electrodes were deposited on a roughened Cu substrate. The substrate had an arithmetic mean roughness (Ra) of 0.5 μm (approximately 18 μm thickness) that was controlled by the following deposition process: the Cu was deposited electrolytically on a large copper roll in an aqueous bath containing a high concentration of $CuSO_4$. This procedure was established by Iljin-Copper Co., Ltd., which provided the roughened Cu foil. A $NaOH/H_2O$ = 1/100 (v/v) solution was used to remove natural oxides from the surface of the Cu foil. Next, the cleaning solution was removed by annealing in a vacuum chamber (at 1.0×10^{-6} Torr) at 100 °C for 30 min. Finally, the chamber was cooled to room temperature.

Si/Ge multi-layer electrodes were deposited sequentially on a Cu substrate using radio frequency (RF) magnetron sputtering with a multi-target system from 3 in.-diameter Si and Ge targets with 99.9% purity (Kojundo Chemical Laboratory Co., Ltd., Japan) in an argon atmosphere with a 7 sccm gas flow rate. The background pressure was 1.0×10^{-6} Torr, and the working pressure was 5.0×10^{-3} Torr. Targets were pre-sputtered for 0.5 h with 40 W RF power for decontamination. The distance between the substrate and the target was 5 cm. The Si/Ge multilayers were deposited sequentially using a constant power density of 5.48 W cm^{-2} on the Si target, and with various power densities on the Ge target to control the thickness of the Ge layer. The deposition times for each target were varied to create different compositions and numbers of layers with a deposition rate of 15 nm min^{-1} at a power density of 5.48 W cm^{-2} on the Si target, and 10 nm min^{-1} at 0.44 W cm^{-2} on the Ge target.

The Si–Ge composite electrodes were deposited using a co-sputtering system with two targets. A power density of 5.48 W cm^{-2} was used on the Si target, and power densities of 0.44, 0.66, 1.32, and 1.98 W cm^{-2} were used on the Ge target. The deposition time was varied to yield different film thicknesses.

The chemical compositions and element distributions of the Si–Ge electrodes were examined using energy-dispersive spectroscopy (EDS). The crystal structure of the electrodes was analyzed by X-ray diffraction (XRD, Rigaku D/Max-2200, Japan) using Cu Kα radiation (λ = 1.5418 Å), high-resolution transmission electron microscopy (HR-TEM, JEM-2100F, JEOL, Japan) with a selected-area electron diffraction (SAED) pattern, and Raman spectroscopy (T64000, ISA Jobin-Y von). The Raman spectra were collected at room temperature using the 541.4 nm line of an argon laser and a 50× magnification microscope on a small selected area (approximately 2 μm^2) of the sample surface. The laser power was maintained at approximately 2 mW. The surface morphologies and topologies of the electrodes were measured using field-emission scanning electron microscopy (FESEM, JES 6340F, Jeol).

To evaluate the electrochemical properties of the Si–Ge films deposited on Cu foil, half cells (CR2032, Hohsen Co., Ltd., Japan) containing the Si–Ge electrode, separator electrolyte, and lithium foil (100 μm thickness, Sigma–Aldrich, Co., Ltd.) as counter electrodes were assembled in a glove box filled with pure Ar. The electrolyte used in the experiments was 1 M $LiPF_6$/ethylene carbonate and dimethyl carbonate (DMC) at a 1:1 volume ratio (Techno Semichem, Co., Ltd.). Cyclic voltammetry (CV) measurements were performed on an electrochemical workstation (WBCS3000, Won A Tech, Co., Ltd., Korea) at a scan rate of 0.01 mV s^{-1} in a potential range of 0.01–1.1 V versus Li/Li$^+$. Galvanostatic charge–discharge half-cell tests were performed at a constant current of 600 μA cm^{-2} (C/5, C being defined as 1 Li$^+$ ion exchanged in 1 h). The test was conducted between the initial OCV and 70 mV versus Li/Li$^+$, then between 70 mV and 1.0 V after the first cycle. For full cell tests, a commercial $LiCoO_2$ cathode, with a capacity of 184.6 mAh g^{-1}, was used as a counter electrode. The electrochemical properties of the full cells were examined at 0.2 C-rates in voltage windows between 3.0 and 4.3 V with the same experimental system. The electrode capacity was calculated according to the weight of the active material.

Ge K-edge X-ray absorption spectra (XAS) of the Si/Ge multilayer for the first and second discharge–charge processes were taken on a BL3C1 (Electrochemistry) beam-line in a storage ring of 2.5 GeV with a ring current of 120–170 mA at the Pohang Light Sources (EXAFS) to study the local structure of the lithiated products. A 13-element Ge detector was installed in the fluorescence detection mode to enhance the sensitivity of the EXAFS signal. The energy range was near the Ge K-edge (11,104 eV), and the sample was maintained at room temperature during the scan. The energy calibration was performed using standard metallic Ge foil. The EXAFS data was analyzed by both conventional [12] and regularization [13] methods. The local structural parameters, such as bond distances, were estimated from the pair distribution function (PDF) determined by the regularization method.

3. Results and discussion

Sixteen Si/Ge multilayer and Si–Ge composite electrodes were prepared with the different Si:Ge ratios and thicknesses as shown in Table 1. The Si/Ge multilayer samples (a1–d4) had 90, 120, and 150 layers with the following ratios: Si:Ge = 7.14:1, 5:1, 2.5:1, and 1.67:1. We assumed that the structure of the multilayer electrode was a composite if the number of layers in the electrode increased to infinity. A mono-layer of more than 150 multilayers was too thin to match the thickness of other samples, so we fabricated an electrode with 90, 120, and 150 layers and a composite. The Si–Ge composited samples were assigned composition ratios according to their atomic percentages. The X-ray diffraction patterns of the as-deposited Si/Ge multilayer and Si–Ge composite electrodes are presented in Fig. 1. The three diffraction peaks from the copper foil were observed at 2θ positions of approximately 43.29°, 50.43°, and 74.13° (JCDPDS 03-1005). There were no peaks related to crystalline Si or Ge. This implies that the RF-sputtered Si–Ge films had an amorphous structure.

Ex situ Raman spectroscopy was used to obtain structural information from the electrodes. The Raman spectra for the Si, Ge, Si/Ge multilayer, and Si–Ge composite films are given in Fig. 1. It has been reported that the Raman peaks of crystalline Si and Ge can be observed at 520 and 303 cm^{-1}, respectively. In the Si/Ge multilayer film Raman analysis, three peaks were observed in the spectra near 274, 390, and 480 cm^{-1}, and each corresponded to an amorphous region of Ge–Ge, Si–Ge, or Si–Si bonds, respectively. The Raman spectra of the Si–Ge composite film were also similar to the spectra of the Si/Ge multilayer film. Therefore, the deposited material prepared in this study was identified to have an amorphous structure. HRTEM is a more effective method to detect the microstructure of thin films. Fig. 2 shows the HRTEM image of the Si–Ge multilayer film. It can be seen that no lattice line appeared in the image. The inset shows the selected-area electron diffrac-

Table 1
Summary of physical properties of Si–Ge binary electrodes: 90, 120, and 150 multilayer and composite system with various ratios of Si and Ge.

Group	Sample	System	Si–Ge monolayer		Thickness
			Si	Ge	
A	a1	90 multilayer	25 nm	3.5 nm	2.56 μm
	a2		25 nm	5 nm	2.7 μm
	a3		25 nm	10 nm	3.15 μm
	a4		25 nm	15 nm	4.05 μm
B	b1	120 multilayer	19 nm	2.5 nm	2.58 μm
	b2		19 nm	3.75 nm	2.73 μm
	b3		19 nm	7.5 nm	3.18 μm
	b4		19 nm	15 nm	4.08 μm
C	c1	150 multilayer	15 nm	2 nm	2.55 μm
	c2		15 nm	3 nm	2.7 μm
	c3		15 nm	6 nm	3.15 μm
	c4		15 nm	12 nm	4.05 μm
D	d1	Composite	$Si_{0.89}Ge_{0.11}$		2.55 μm
	d2		$Si_{0.84}Ge_{0.16}$		2.7 μm
	d3		$Si_{0.73}Ge_{0.27}$		3.15 μm
	d4		$Si_{0.58}Ge_{0.11}$		4.05 μm

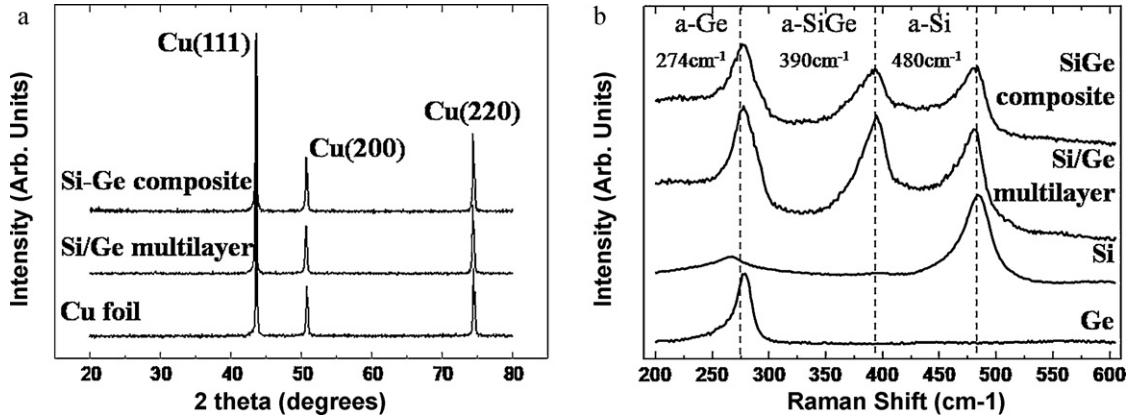

Fig. 1. (a) XRD patterns of Cu foil, Si/Ge 120 multilayer with Si 19 nm and Ge 15 nm, and $Si_{0.58}Ge_{0.42}$ composite electrodes deposited rough Cu foil and (b) Raman spectra of as-deposited Si, Ge, Si/Ge multilayer, and Si–Ge composite electrodes.

tion (SAED) pattern taken from the deposited film. The pattern is dispersed and very ambiguous. This indicates that the Si–Ge film existed only in amorphous structure. An amorphous structure is typically more open than a well-crystallized one. It has been recognized that amorphous materials exhibit homogeneous volume expansions/contractions during charge/discharge and a relatively open structure would adequately prevent the lattice from expanding and provide more diffusion paths for Li ions [14].

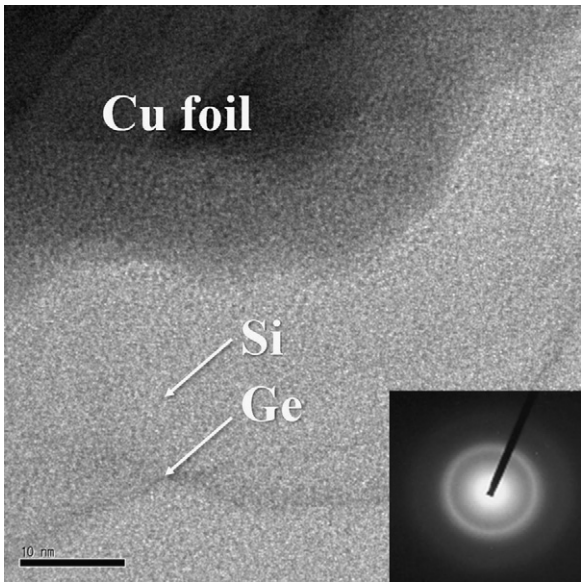

Fig. 2. TEM image and corresponding SAED pattern (inset) of as-deposited Si/Ge multilayer electrode prepared by RF/DC magnetron sputtering.

Fig. 3 shows the morphology of the Si–Ge electrode film in field emission scanning electron microscopy (FE-SEM) and high-resolution transmission electron microscopy (HR-TEM) images taken at different magnifications. As shown from TEM images in Fig. 3(a)–(c), the Si/Ge multilayer electrodes had a laminate structure. In the Si/Ge 120 multilayer films (Fig. 3(a)), the structure was composed of a Si layer with a thickness of 19 nm and a Ge layer with a thickness of 2.5 nm, the Si/Ge 150 multilayer had a 19 nm Si layer, and a 3 nm Ge layer, as shown in Fig. 3(c). Alternatively, the Si–Ge composite film with a thickness of 2.7 μm had an undistinguished structure (SEM image in Fig. 3(d)) with uniform thickness. Fig. 3(e) and (f) shows the plane morphologies of the electrolytically deposited Cu foil and Sample c2 (Si/Ge film deposited on electrodeposited Cu foil). The surface of the Cu foil contained many irregularities that increased the adhesion force between the deposited film and foil, and provided many Li^+ diffusion paths by increasing the surface area of the film.

The Li^+ insertion/extraction reactions of the Si–Ge electrodes were studied by cyclic voltammetry (CV), which measures the electrical potential over the region where the main reaction of an electrode occurs. The CVs of the Si, Ge, Si/Ge 150 multilayer, and Si–Ge composite were measured between 0.01 and 1.1 V at slow scan rates of 0.01 mV s^{-1}, as shown in Fig. 4. The potential was determined to occur over a wider range (from 0.01 to 1.1 V) than

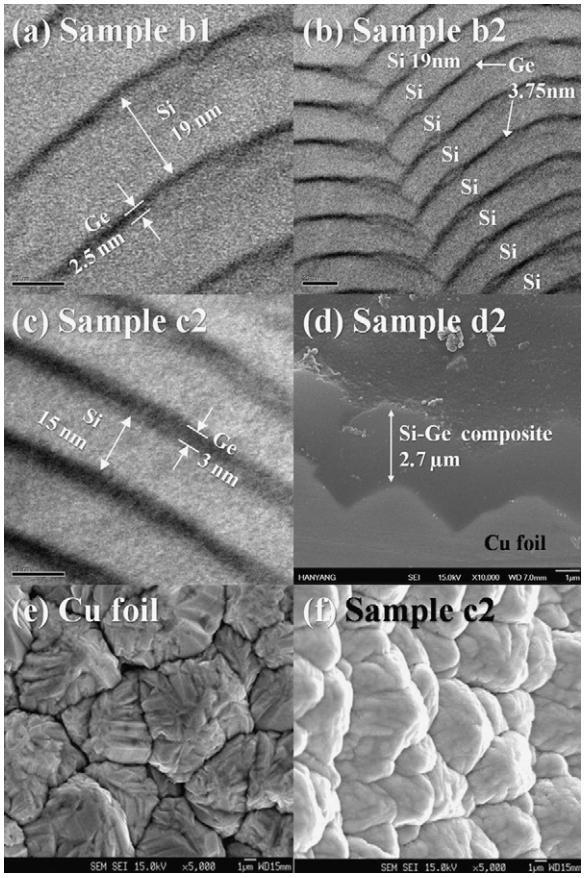

Fig. 3. TEM images of cross-section image of (a) Si/Ge multilayer with Si 19 nm and Ge 2.5 nm (Sample b1), (b) Si/Ge multilayer with Si 19 nm and Ge 3.75 nm (Sample b2), (c) Si/Ge multilayer with Si 15 nm and Ge 3 nm (Sample c2), (d) $Si_{0.84}Ge_{0.16}$ composite film with 2.7 μm thickness, and SEM images of (e) Cu foil and (f) as-deposited Sample c2.

the existing test potential (from 0.1 to 1.0 V) because the potential range is too complex due to the two active materials with lithium ions. In the Si and Ge scans, currents caused by the oxidation reactions of Si (Fig. 4(a)) and Ge (Fig. 4(b)) were observed in the 0.15–0.2 V [15] and 0.3–0.4 V [16] regions, respectively. In the reduction reaction regions, the current peaks of Si and Ge were similar for the potential region at approximately 0.6 V. In the reduction region of Ge at 0.6 V, the current peak can be attributed to SEI formation, as reported by Billiard [16]. Weydanz et al. [17] reported that an anodic peak of 0.58 V indicates the equilibrium potential values of $Si/Li_{12}Si_7$ for the solid system. This difference can originate from different equilibrium potentials, which are related to different material structures and defect densities. This experiment was repeated under the same conditions for Samples c2 and d2. It was assumed that these samples represented Si/Ge multilayer and Si–Ge composite anodes. The two CVs of the electrodes are shown in Fig. 4(c) and (d). There are two similar sets of broadened cathodic peaks at 0.01–0.2 V and broadened anodic peaks at 0.5–0.7 V in both electrodes. These peaks were attributed to the potential dependent reactions between different alloy phases related to the Si–Li and Ge–Li alloys/de-alloys. The cycle performances of Si and Ge electrodes are shown in the insets of Fig. 4(a) and (b). They show that Si had a high initial discharge capacity of approximately 2500 mAh g^{-1}; however this was an acute capacity. As mentioned in Section 1, Ge has limited usefulness as an anode material, due to its cost, although it had an initial discharge capacity of approximately 1200 mAh g^{-1} and a steady cycle performance, as shown in the inset of Fig. 4(b).

A constant current test was conducted to measure the charge and discharge characteristics of each electrode. Fig. 5 shows the discharge capacities of the Si–Ge electrodes as a function of the cycle number. The cells were cycled between 0.01 and 1.1 V versus Li/Li^+ at a current density of 600 μA cm^{-2}. The performances of all 16 batteries were tested, and the influences of two parameters (ratios of Si and Ge, system of electrodes: 90, 120, and 150 multilayer, composite) were investigated.

Four samples of each system with different Si and Ge ratios were compared: Fig. 5(a) shows the cycle performance of the Si/Ge 90 multilayer with a thickness ratio of Si:Ge = 25 nm:3.5 nm, Si:Ge = 25 nm:5 nm, Si:Ge = 25 nm:10 nm, and Si:Ge = 25 nm:20 nm. The ratios of Si and Ge in other systems were similar to the Si/Ge 90 multilayer anode shown in Fig. 5(b)–(d).

The four electrode systems were investigated to understand the effects of the multilayer and composite structures. For example, the Si and Ge thickness ratios of Samples a4, b4, and c4 were 5:1. The volume ratio of Si and Ge was maintained at approximately 5:1 by controlling the plasma power density during sputtering according to the deposition rates of each target (Si, Ge), although the Si and Ge thickness ratios of Sample d4 were not calculated due to the composite system.

To simply analyze two parameters, the initial discharge capacities and capacity retention rates at 100 cycles were summarized (Fig. 5(e)). Four batteries (b1, b2, b3, and b4) were made using 90 multilayer systems. Results showed that the increased Ge content in the Si/Ge multilayer gradually decreased the discharge capacity of the four samples, because Ge has a smaller specific capacity than Si. The capacity retention rates during 100 cycles of the samples increased until b2, and slightly decreased from b2 to b4 because the thicknesses of the samples gradually increased along with the increasing Ge content in the film. Capacity fade commenced more rapidly and continued to steadily fade, due to more intercalation-induced stress in the thicker films [7]. During preparation of the samples, the thickness of Si in the first Si/Ge layer was the same in all samples to simplify analysis. The total thicknesses of all Si–Ge electrodes were not the same, although it was tried to match the total thicknesses of all samples. However, the effect of the multilayer dramatically declined in Samples b4, c4, and d4, even considering their increasing thicknesses that accelerated the capacity fade. In our previous results [18], the electrode with a thickness greater than 3 μm showed sharp degradation, although it had improved cycleability. It is unclear whether the thickness effect was a disadvantage for the capacity fade. Other sample groups (C and D) showed similar tendencies. However group A (a4) showed a different behavior than other groups (b4, c4, and d4) for cycleability. It suggests that the inter-metallic matrix of Si and Ge were formed and supplemented the shortcomings of the thick electrode. In the multilayer groups (B, C, and D), it was assumed that the effect of the Si–Ge multilayer declined as the total thickness increased according to the increasing Ge layer. From this result, it is suggested that the ratio of Si to Ge was suitable at 2.5–5:1, with a thickness less than 3.15 μm. We then compared electrode systems: Set 1 (a1, b1, c1, and d1), Set 2 (a2, b2, c2, and d2), Set 3 (a3, b3, c3, and d3), and Set 4 (a4, b4, c4, and d4). Set 1 consisted of four batteries (a1, b1, c1, and d1). For these samples, the initial discharge capacities were 2092, 2026, 2100, and 1915 mAh g^{-1}, and the capacity retention rates after 100 cycles were 47, 72.7, 74.3, and 70.8%, respectively. The initial discharge capacities of the four samples were similar; however, the capacity retention rate of Sample a1 was quite different. This distinct trend was observed for all sets. Considering the Si/Ge 90 multilayer system, the cycle performance was less advanced than for the 120 multilayer, 150 multilayer, or composite systems, although the specific capacity was sufficiently improved to replace conventional carbon. The reason for the difference in cycle performance was unclear; however

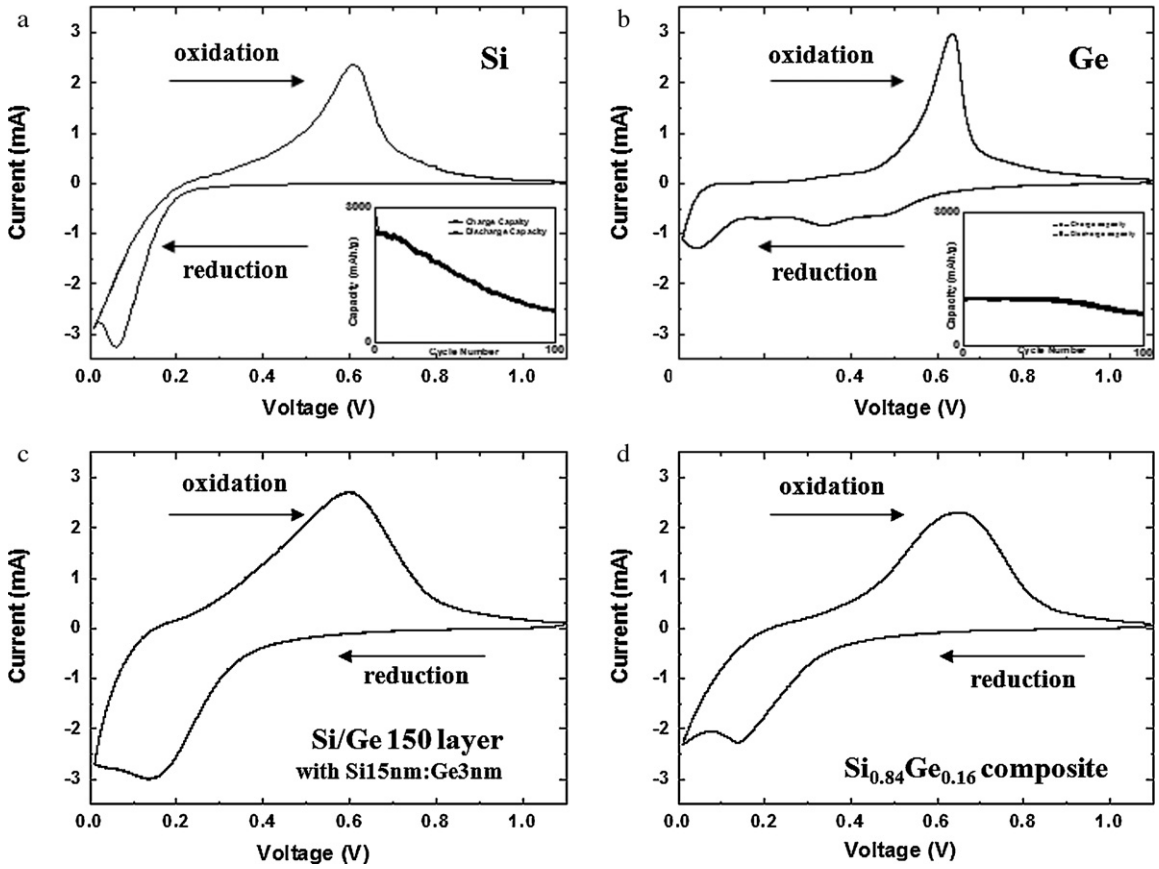

Fig. 4. Cyclic voltammetry (CV) plots of (a) Si, (b) Ge, (c) Si/Ge 150 multilayer with Si 15 nm and Ge 3 nm, (d) $Si_{0.84}Ge_{0.16}$ composite, and cycle performance of Si (inset of (a)) and Ge (inset of (b)).

it was likely due to the differences in film structures. The number of 90 Si/Ge layers did not prevent capacity fade, unlike the 120 and 150 multilayers, or the composite system. However, there was sufficient distribution of the intercalation-induced stress over the 90 Si/Ge layers during lithium ion insertion/extraction. Sakai and co-workers [19] reported that the improvement in cycle performance was due to the prevention of mechanical fracture in the film caused by the dispersion of the intercalation-induced stress. Unlike the 90 multilayer, the 120 multilayer, 150 multilayer, and composite system were effective. It was assumed that the composite system would act as a multilayer system with an infinite number of layers, since a single Ge layer in the film should consist of a thickness less than 2 nm over the 150 layer system. The three systems showed similar cycle performances, as shown in Fig. 5(b)–(d).

Among the 16 samples tested, Samples b2, c2, and d2 with a 5:1 ratio of Si to Ge showed excellent specific capacities and cycle performances. To investigate the electrochemically lithiated Si and Ge in these three samples, the XRD patterns of as-deposited and lithiated material after 10 cycles were analyzed to find lithium alloys. Fig. 6 displays the XRD patterns of Samples b2, c2, and d2 with their lithium alloy species. The crystalline structures of the different Li_xSi_y and Li_xGe_y are indicated as closed and open shapes, respectively. Both the as-deposited sample and the lithiated sample of each electrode were compared. As shown in all of the plots, some crystalline $Li_{12}Si_7$, Li_2Si_1, $Li_{21}Si_8$, and Li_7Si_2 peaks were generated after lithiation by alloying the lithium ions with Si. However, Li–Ge alloy peaks appeared with different patterns. In Sample b2 (Fig. 6(a)), which consisted of 120 layers (Si: 19 nm, Ge: 3.75 nm), some $Li_{11}Ge_6$ and Li_7Ge_2 peaks were generated. Some of the Li–Ge peaks did not appear or appear with small intensities for Samples c2 and d2. The XRD peaks for Sample c2 (Fig. 6(b)) were similar to those of Sample b2, but one peak did not appear or appeared only slightly. A few Li–Ge peaks corresponding to $Li_{11}Ge_6$ and Li_7Ge_2 appeared for Sample d2 with the composite system (Fig. 6(c)). These results suggest that such differences could have influenced the cyclability of the cell. Ge, which was not alloyed with Li-ions, acted as an inactive material and as a mechanical buffer against electrode pulverization caused by the large volume expansion. This can be attributed to the fact that, while the Si/Ge 150 multilayer resulted in an effective aspect ratio for the Si–Ge electrodes, the reversible lithium ions in the Ge layers were attributable, in part, to a diffusivity greater than Si [20], which provided a higher reversible cycle performance.

To evaluate the effects of Ge, EXAFS analysis was performed on Sample c2, as its capacity retention rate was the most noticeable of the sixteen samples. Fig. 7 shows a comparison of the normalized Ge K-edge XANES spectra for the Ge metallic film, Sample c2 (as-deposited Si/Ge 150 multilayer with Si 15 nm:Ge 3 nm), and the first and second discharges/charges of Sample c2. The main absorption by the Ge–Ge bonds appeared at 11,110 eV. However, the main absorption by the Si–Ge bonds shifted to 11,105 eV [21,22] by the addition of Si. The peak broadened and its position shifted to 11,107 eV from the first discharge to 0.01 V, however the peak returned to the original position and shape at 11,105 eV. This trend was also observed at the second charge and discharge. The full intergradations of the Si–Ge bonds did not occur, although the Si–Ge bonds were somewhat changed by the Li-ion insertion/extraction to the electrode. Therefore the interfaces of Si and Ge may be suppressed by the breakaway of active materials. Cho et al. [23] reported that a weak absorption peak at this energy can be explained by the small particle size of pristine Ge. Since the elec-

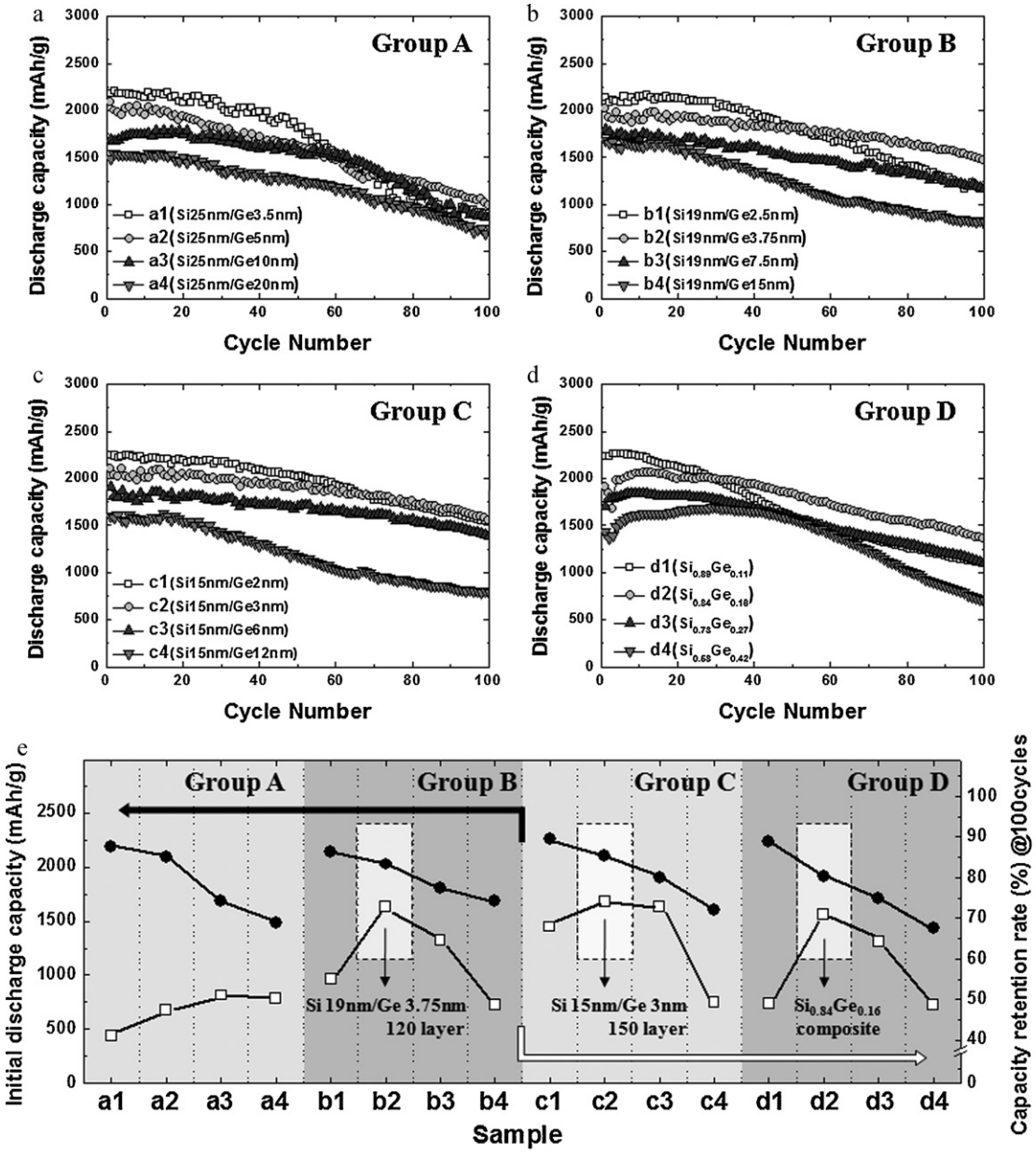

Fig. 5. Cycle performances of sixteen electrodes with multilayer or composite system: (a) Si/Ge 90 multilayer, (b) Si/Ge 120 multilayer, (c) Si/Ge 150 multilayer, (d) Si/Ge 90 multilayer with various ratios of Si and Ge, and (e) comparisons of tested sixteen samples at initial discharge capacities and capacity retention rate during 100 cycles.

tronic configuration of the Ge metallic phase is [Ar] $3d^{10}4s^24p^2$, the peak intensity of the Si/Ge electrode is related to the concentration of the 4p hole state. Compared with the peak feature of the bulk metallic phase, the decrease in the peak intensity of the other phases was the result of the decrease in the p character in the 4p level. The peak feature variation seen in the NEXAFS results can be explained by the small size, as compared to the metallic Ge particle size.

The EXAFS characterization at the Ge K-edge shows effective local structural variation of Li-ion behavior near the Ge atom. Fig. 8 shows the Fourier transform (FT) magnitudes of the Ge K-edge *k*-weighted EXAFS spectra for the Ge metallic film, and those after the first and second discharges and charges of Sample c2. For the Ge metallic film, a characteristic peak at ~1.8 Å corresponds to the Ge–Ge bonds of Ge metal. Alternatively, Sample c2 shows a strong peak evolution at ~1.9 Å, believed to be Ge–Ge bonds from Si–Ge interactions. Upon discharging to 0.01 V at the first cycle, the average Ge–Ge bond distance of the Si/Ge electrode increased by approximately 0.35 Å with respect to that of the pristine case. The peak of the first discharged sample shows a characteristic peak at 2.25 Å related to the position of the Ge–Ge bonds expanded by the lithium ion. The Li ion position in the active materials led to a local structural modification near the central Ge atom. On the first charge to 1.1 V, the peak shown at 2.02 Å corresponds to the Ge–Ge phase recovered as the Li was extracted. The peak at 2.02 Å shifted to the right with respect to the Ge–Ge bonds of the as-deposited Si/Ge phase, which indicates that the Ge structure expanded slightly at 1.1 V.

The reaction mechanism during the second cycle was similar to that of the first cycle. However, when the electrode materials reacted with Li, the intensity of the peak at 2.25 Å decreased, as the potential decreased to less than that in the first cycle. On the second charge to 1.1 V, the peak at 2.02 Å reversibly returned to that of the peak position of the first charge state, and the intensity of

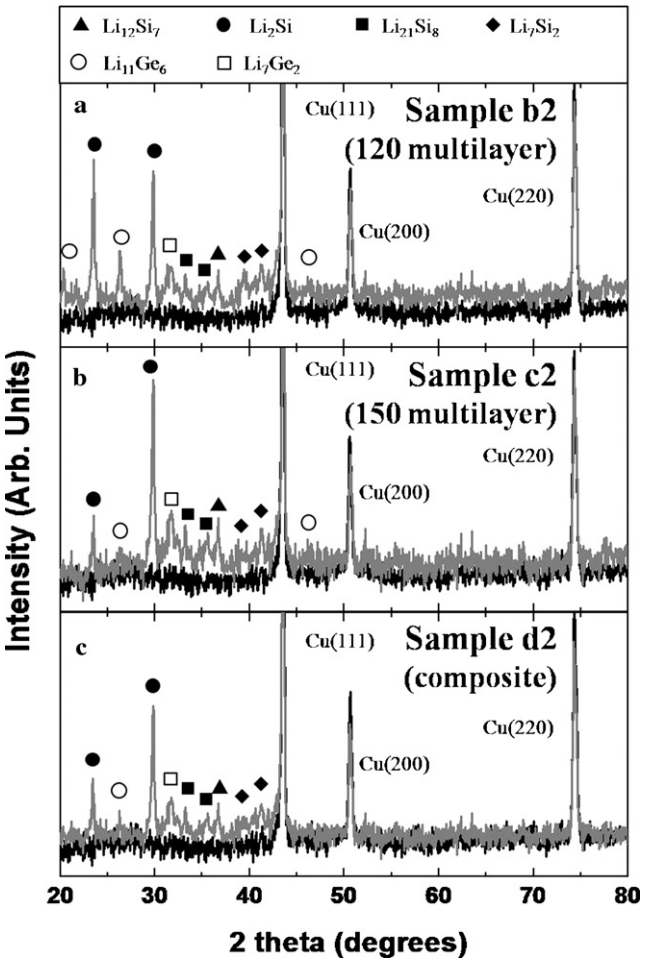

Fig. 6. XRD patterns of Si/Ge multilayer and Si–Ge composite electrodes as charge state after 10 cycles: (a) Si/Ge 120 multilayer with Si 19 nm and Ge 3.75 nm, (b) Si/Ge 150 multilayer with Si 15 nm Ge 3 nm, and (c) $Si_{0.84}Ge_{0.16}$ composite electrode.

the peak decreased abruptly. This small peak [24] may be due to the Ge–Ge bonds in metallic Ge and indicated Ge in the Si/Ge film. The Ge–Ge bonds of the metallic Ge and Si–Ge bonds may have been lengthened by disordering the structure during lithium ion insertion/extraction into the electrode. This result clearly shows

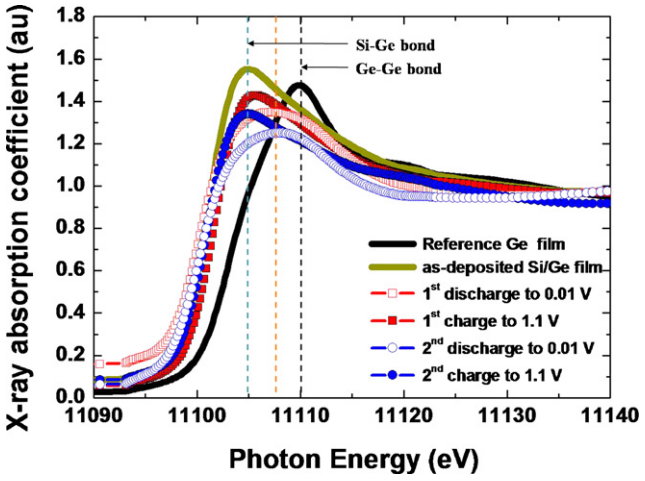

Fig. 7. Normalized Ge K-edge XANES spectra for metallic Ge film, as-deposited Si/Ge multilayer film (Sample c2), first and second-discharge to 0.01 V and charge 1.1 V of the Si/Ge multilayer electrode.

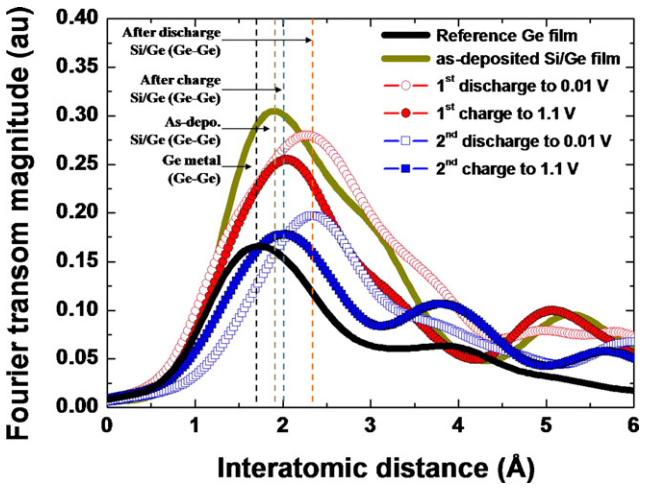

Fig. 8. Fourier transform (FT) magnitudes of the Ge K-edge *k*-weighted EXAFS spectra for metallic Ge film, as-deposited Si/Ge multilayer film (Sample c2), first and second-discharge to 0.01 V and charge 1.1 V of the Si/Ge multilayer electrode.

that the electrochemical behavior of the Si/Ge multilayer for Li was reversible during the cycle due to the maintenance of the Si–Ge bonds. Thus, the Si–Ge bonds were not broken when Li was inserted and extracted from the Si/Ge phase during the cycle. These results suggest that the interface of Si and Ge was capable of accommodating the volume expansion during charge–discharge cycling by maintaining the Si–Ge bonds.

Full cells coupled with commercial $LiCoO_2$ cathodes were assembled to test the practical application of Si–Ge electrodes in lithium rechargeable batteries. The anode/cathode capacity ratios were ~1.5:1. Fig. 9(a)–(c) shows the required negative/positive capacity ratio to optimize the capacity and increase the performance of the three Si–Ge system anodes coupled with the $LiCoO_2$ cathodes in the full cell. The charge capacity of $LiCoO_2$ as a cathode was 2.4 mAh (184.6 mAh g^{-1}) and the irreversible capacity was 0.36 mAh (27.7 mAh g^{-1}). In Fig. 9(a), when the Si/Ge 120 multilayer electrode (Si: 19 nm, and Ge: 3.75 nm) was used as a negative electrode, the charge capacity was ~3.6 mAh (2099.7 mAh g^{-1}), the irreversible capacity was 0.13 mAh (74.1 mAh g^{-1}), and the negative/positive capacity ratio (N/P ratio) was 1.5 (3.63 mAh/2.4 mAh = 1.5). In Fig. 9(b), the charge capacity of the Si/Ge 150 multilayer electrode (Si: 15 nm, Ge: 3 nm) as an anode was ~3.7 mAh (2195.8 mAh g^{-1}), the irreversible capacity was 0.16 mAh (96.1 mAh g^{-1}), and the N/P ratio was 1.54, which is similar to that of the Si/Ge 120 multilayer/$LiCoO_2$ cell shown in Fig. 9(a). Finally, the $Si_{0.84}Ge_{0.16}$ composite electrode (Fig. 9(c)), when used as an anode, showed the discharge capacity of ~3.5 mAh (2015.3 mAh g^{-1}), the irreversible capacity of 0.14 mAh (74.5 mAh g^{-1}), and the N/P ratio was also 1.5. Fig. 9(d) shows the results of the galvanostatic cycling experiments of the three cells. The cells were cycled in the potential range of 3–4.3 C, with a cycling rate of approximately 0.2 C with respect to $LiCoO_2$. This yields a comparison of the cycling performance of the Si/Ge 120 multilayer anode/$LiCoO_2$, the Si/Ge 150 multilayer anode/$LiCoO_2$, and the $Si_{0.84}Ge_{0.16}$ composite anode/$LiCoO_2$.

Table 2 summarizes the initial capacities, coulombic efficiencies, and cycle retentions of the half and full cells with Samples b2, c2, and d2 as anodes and $LiCoO_2$ as the cathode. During the first discharge, the $Si_{0.84}Ge_{0.16}$ composite/$LiCoO_2$ full cell delivered a specific discharge capacity of approximately 213.7 mAh g^{-1} (calculated according to the cathode mass of $LiCoO_2$) and a cycle retention after 100 cycles of 52.4%. It appears that the improvement in the Li-ion capacity and cycle performance of the $Si_{0.84}Ge_{0.16}$ composite electrodes was primarily due to the effective proportion of the

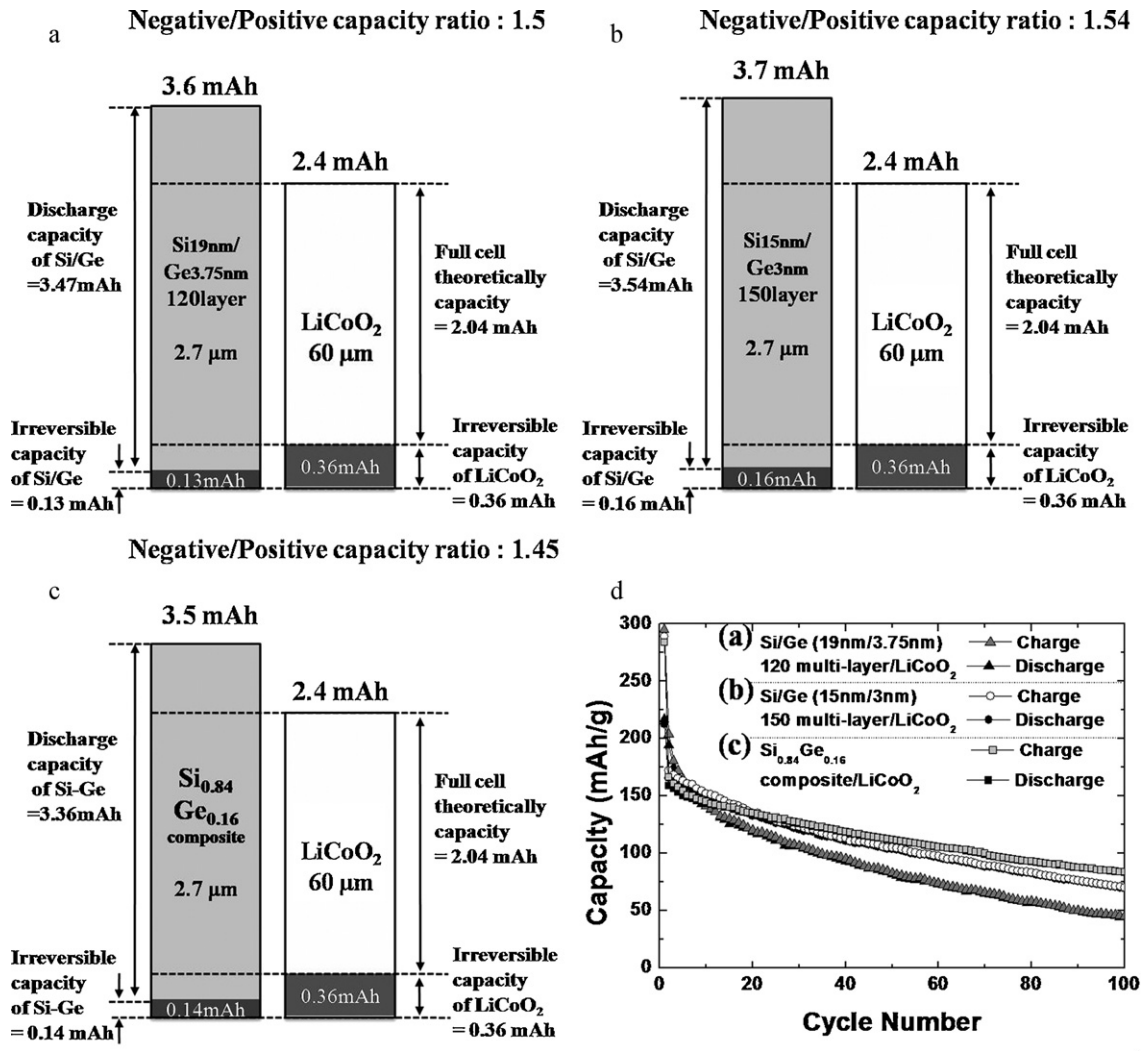

Fig. 9. Mimetic diagrams of full cell combined with LiCoO2 cathode and (a) Si/Ge 120 multilayer with Si 19 nm and Ge 3.75 nm, (b) Si/Ge 150 multilayer with Si 15 nm and Ge 3 nm, and (c) Si0.84Ge0.16 composite anode and negative/positive capacity ratio of three full cells is about 1.5:1. (d) And cycle performances of the full cell (a), (b), and (c). Voltage window and current density were 4.3–3.0 V versus Li/Li^+ and 275 μA cm^{-2}.

Ge element in the film and the structures of the films. The Si/Ge 120 multilayer/$LiCoO_2$ and Si/Ge 150 multilayer/$LiCoO_2$ full cells showed discharge capacities of 217.2 and 213 mAh g^{-1}, and capacity retentions of 22.8 and 42.2%, respectively.

These results indicate that the experimental conditions were not optimized for the Si-based anodes, as these experimental conditions have been used for commercial carbon anodes. However, the multilayer and composite systems containing Ge for diversifying the structures of the films showed slightly higher cycle stabilities and improved electrochemical performances in the full cells. The two parameters (ratio of Si to Ge, and electrode system: 90, 120, and 150 multilayer, composite) of the Si–Ge binary electrodes provided a new level for examining the synthetic materials to replace carbon. Additionally, the proposed Si–Ge binary electrodes can be

Table 2
Summary of the results of (a) Sample b2 (Si/Ge 120 multilayer with Si 19 nm and Ge 3.75 nm)/Li and Sample b2/$LiCoO_2$ full cell, (b) Sample c2 (Si/Ge 150 multilayer with Si 15 nm and Ge 3 nm)/Li and Sample c2/$LiCoO_2$ full cell, and (c) Sample d2 ($Si_{0.84}Ge_{0.16}$ composite)/Li and Sample c2/$LiCoO_2$ full cell.

$LiCoO_2$ (cathode) +Si-Ge (anode)	Initial charge capacity		Initial discharge capacity		Cycle retention @100 cycles (%)	1st cycle efficiency (%)	Average Coulombic efficiency @100 cycles (%)
	mAh	mAh/g	mAh	mAh/g			
$LiCoO_2$	2.4	184.6	2.04	156.9	84	85	98.9
(a) Sample b2							
Half cell	3.6	2099.7	3.47	2025.6	72.7	96.5	99.5
Full cell	3.83	295.2	2.82	217.2	22.8	73.6	98.6
(b) Sample c2							
Half cell	3.7	2195.8	3.54	2099.7	74.25	95.6	99.4
Full cell	3.75	289	2.77	213	42.2	73.7	98.3
(c) Sample d2							
Half cell	3.5	2015.4	3.36	1915.3	70.8	95.1	99.6
Full cell	3.7	284.3	2.78	213.7	52.4	75.2	99.1

applied in electrical appliances, especially in high-density power supplies, due to their smaller mass and volume of active materials, when compared to commercial carbon.

4. Conclusions

This work demonstrated that the use of the active element germanium in the multilayer or composite systems with a Si-based anode was an efficient way to improve the electrochemical properties of Si–Ge binary system electrodes. This outcome was attributed to improvements in the cycle stability. Amorphous Si–Ge binary electrodes were prepared by RF/DC magnetron sputtering. The ratio of Si to Ge was determined and the suitable systems (multilayer or composite) were evaluated for use as electrodes. A Si/Ge 150 multilayer structure (Si: 15 nm, Ge: 3 nm)/Li half cell exhibited a remarkable discharge capacity of approximately 2100 mAh g^{-1} and a noteworthy cycle retention rate of 74.25%. A $Si_{0.84}Ge_{0.16}$ composite anode, coupled with $LiCoO_2$ as a cathode full cell, showed an initial discharge capacity of 213 mAh g^{-1} and a cycle retention rate of 52.4% over 100 cycles. These results suggest that sputtered Si–Ge binary electrodes are promising anode materials for next generation lithium ion batteries.

Acknowledgements

This work was financially supported by the Korean Science and Engineering Foundation (KOSEF) through the Research Center for Energy Conversion and Storage and by the Brain Korea 21 Project under the Ministry of Education and Human Resources Development, Republic of Korea.

References

[1] U. Kasavajjula, C. Wang, A.J. Appleby, J. Power Sources 163 (2007) 1003.
[2] C.J. Wen, R.A. Huggins, J. Solid State Chem. 37 (1981) 271.
[3] I.-S. Kim, P.N. Kumta, J. Power Sources 136 (2004) 145.
[4] J. Graetz, C.C. Ahn, R. Yazami, B. Fultz, J. Electrochem. Soc. 151 (2004) A698.
[5] J.K. Lee, M.C. Kung, L. Trahey, M.N. Missaghi, H.H. Kung, Chem. Mater. 21 (2009) 6.
[6] T.D. Hatchard, M.N. Obrovac, J.R. Dahn, J. Electrochem. Soc. 153 (2006) A282.
[7] J.P. Maranchi, A.F. Hepp, A.G. Evans, N.T. Nuhfer, P.N. Kumta, J. Electrochm. Soc. 153 (2006) A1246.
[8] Y.L. Kim, H.Y. Lee, S.W. Jang, S.H. Lim, S.J. Lee, H.K. Baik, Y.S. Yoon, S.M. Lee, Electrochim. Acta 48 (2003) 2593.
[9] J.P. Maranchi, A.F. Hepp, P.N. Kumta, Electrochem. Solid-State Lett. 6 (2003) A198.
[10] M.-H. Kim, Y.-J. Kim, Y.-K. Lee, J.A. Ascencio, J.-W. Park, Rev. Mex. Fis. S53 (1) (2007) 17.
[11] C.-M. Hwang, C.-H. Lim, J.-H. Yang, J.-W. Park, J. Power Sources 194 (2009) 1061.
[12] D.C. Koningsberger, R. Prins, X-ray Absorption: Principles, Applications, Techniques of EXAFS, SEXAFS and XANES, Wiley Interscience, New York, 1988.
[13] D.-S. Yang, J.M. Lee, Phys. Scr. T115 (2005) 200.
[14] R. Motooka, O.W. Holland, Appl. Phys. Lett. 58 (1991) 2360.
[15] K.L. Lee, J.Y. Jung, S.W. Lee, H.S. Moon, J.W. Park, J. Power Sources 129 (2004) 270.
[16] B. Laforge, L. Levan-Jodin, R. Salot, A. Billiard, J. Electrochem. Soc. 155 (2008) A181.
[17] W.J. Weydanz, M. Wohlfahrt-Mehrens, R.A. Huggins, J. Power Sources 81–82 (1999) 237.
[18] C.-M. Hwang, J.-W. Park, Thin Solid Films 518 (2010) 6590.
[19] J. Yin, M. Wada, K. Yamamoto, Y. Kitano, S. Tanase, T. Sakai, J. Electrochem. Soc. 153 (3) (2006) A472.
[20] J. Graetz, C.C. Ahn, R. Yazami, B. Fultz, Electrochem. Solid-State Lett. 6 (2003) A194.
[21] O. Majerus, L. Cormier, J.P. Itie, G. Calas, Phys. Scr. T115 (2005) 525.
[22] N. Sung, Y.G. Yoo, D.S. Yang, AIP Conference Proceedings, vol. 882, 2007, p. 566.
[23] H. Lee, M.G. Kim, C.H. Choi, Y.-K. Sun, C.S. Yoon, J.P. Cho, J. Phys. Chem. B 109 (2005) 20719.
[24] S.I. Lee, S.K. Yoon, C.M. Park, J.-M. Lee, H.S. Kim, D.M. Im, S.-G. Doo, H.-J. Sohn, Electrochim. Acta 54 (2008) 364.